American Mineralogist, Volume 96, pages 974–982, 2011

A first-principles study of the phase transition from Holl-I to Holl-II in the composition $KAlSi_3O_8$

Liwei Deng,[1] Xi Liu,[1,*] Hong Liu,[2] and Yigang Zhang[3]

[1]The Key Laboratory of Orogenic Belts and Crustal Evolution, Ministry of Education of China, School of Earth and Space Sciences, Peking University, Beijing 100871, China
[2]Institute of Earthquake Science, China Earthquake Administration, Beijing 100036, China
[3]State Key Laboratory of Lithospheric Evolution, Institute of Geology and Geophysics, Chinese Academy of Sciences, Beijing 100029, China

Abstract

The phase relation and structural evolution of Holl-I and Holl-II in the composition $KAlSi_3O_8$ at 0 K have been investigated by the first-principles method up to 130 GPa. Holl-I and Holl-II are polymorphs of $KAlSi_3O_8$ stable at low pressures and high pressures, respectively. The transition pressure is determined at ~23(5) GPa, in agreement with recent experimental observations. All experimentally observed major changes associated with this phase transition such as the deviation of the γ-angle from 90°, splitting of the *a*- and *b*-axes, as well as its *P*-*V* evolution, are successfully simulated. By evaluating the effect of different Al/Si substitution mechanisms on the computing cell of Holl-I, we have found: (1) different Al/Si substitution mechanisms do not result in apparent difference in the minimized cohesive energies, suggesting a possible random distribution of Al and Si; (2) different Al/Si substitution mechanisms lead to different powder X-ray diffraction features, which, compared to the experimentally observed powder X-ray diffraction data, implies that local non-random distribution of Al and Si exists to some extent in the Holl-I structure; and (3) the phase transition from Holl-I to Holl-II might be associated with a change in the distribution pattern of Al and Si in the structure. From the simulated compression data, we have derived K_0 = 174 GPa and V_0 = 244.82 Å^3 for Holl-I, and K_0 = 168 GPa and V_0 = 244.8 Å^3 for Holl-II (K_0' fixed at 4). The larger K_0 of Holl-I is probably related to the more stable squared open tunnel delimited by the rigid tetragonal octahedral framework, which is gradually deformed by compression in Holl-II after the phase transition from Holl-I to Holl-II.

Keywords: Equation of state, first-principles simulation, Holl-I, Holl-II, phase transition

Introduction

Feldspar is one of the dominant phases in the Earth's upper continental crust and may be carried from the Earth's surface down to the Earth's interior via the subduction process (Dupre and Allegre 1983; Hofmann 1997; Bozhilov et al. 1999; Hirose et al. 1999; Liu et al. 2007; Wu et al. 2009). As demonstrated by some high-*P* experiments up to about 24 GPa (Irifune et al. 1994), the proportion of its high-*P* form, mainly $KAlSi_3O_8$-hollandite, could volumetrically account for one third of the phase assemblages of the subducted upper continental crust composition, so that its importance in the geodynamic process in the deep interior of the Earth cannot be overestimated. Orthoclase (Or; $KAlSi_3O_8$) is one of the major end-members in the feldspar family, and its high-*P* behavior is of great interest to many investigators (e.g., Yamada et al. 1984; Zhang et al. 1993; Urakawa et al. 1994; Yagi et al. 1994; Tutti et al. 2001; Akaogi et al. 2004; Sueda et al. 2004; Nishiyama et al. 2005; Liu 2006; Ferroir et al. 2006; Yong et al. 2006; Liu and El Goresy 2007; Hirao et al. 2008; Liu et al. 2009).

Previous studies have generally reached good agreements on the phase relations of the composition $KAlSi_3O_8$ up to the pressure of 128 GPa (Urakawa et al. 1994; Yagi et al. 1994; Tutti et al. 2001; Akaogi et al. 2004; Sueda et al. 2004; Nishiyama et al. 2005; Liu 2006; Ferroir et al. 2006; Yong et al. 2006; Liu and El Goresy 2007; Hirao et al. 2008; Liu et al. 2010). First, Or ($KAlSi_3O_8$) breaks down to a three-phase assemblage (wadeite-type $K_2Si_4O_9$ + kyanite-type Al_2SiO_5 + SiO_2) at around 6 GPa and 600–1400 °C. Second, these three phases recombine to form a hollandite-type phase with the composition $KAlSi_3O_8$ (Holl-I hereafter) at about 9–10 GPa and 1000–1500 °C. Third, Holl-I transforms to a structurally modified hollandite-like phase (Holl-II; $KAlSi_3O_8$) at about 23–25 GPa and 500–1500 °C. Finally, Holl-II possibly remains thermodynamically stable up to 128 GPa. Mainly due to its unquenchable nature during decompression, Holl-II was difficult to detect within experimental products generated by traditional high-*P* quench methods, so that some discrepancy in the phase transition from Holl-I to Holl-II was reported (Tutti et al. 2001; Sueda et al. 2004; Nishiyama et al. 2005; Ferroir et al. 2006).

Holl-I has tetragonal symmetry *I*4/*m* (Ringwood et al. 1967; Yamada et al. 1984), whereas Holl-II has monoclinic symmetry

* E-mail: xi.liu@pku.edu.cn

*I*2/*m* (Sueda et al. 2004; Nishiyama et al. 2005; Ferroir et al. 2006). Paired edge-sharing $(Si,Al)O_6$ octahedra form double chains running parallel to the *c*-axis, and four of the double chains are linked to delimit a large squared open tunnel to host the K cation. High-pressure experiments have demonstrated that many geochemically important large radius cations such as Na, Ca, Sr, and Rb can be hosted by the Holl-I structure (Rapp et al. 2008). Since the structure of Holl-II is different to the one of Holl-I, its capability in hosting the large radius cations might be very different as well. Consequently, it is geochemically very important to investigate this phase transition down to the atomic level.

Yet, Holl-II is unquenchable and quickly converts to Holl-I during pressure release (Sueda et al. 2004; Nishiyama et al. 2005; Ferroir et al. 2006), so that traditional high accuracy single-crystal X-ray diffraction on quenched synthesized single crystal cannot be used to explore its structural details. Ab initio simulation has unparalleled advantages in exploring information associated with unquenchable high-pressure phase transitions, and this technique has been widely applied to phase transitions of different types (e.g., Waghmare and Rabe 1997; Meng et al. 2004; Iitaka et al. 2004; Martinez and Durandurdua 2006; Durandurdua 2009a, 2009b). For the composition $KAlSi_3O_8$, three theoretical calculations have been carried out so far (Winkler et al. 2002; Mookherjee and Steinle-Neumann 2009a; Caracas and Boffa Ballaran 2010). Winkler et al. (2002) mainly developed a new method to investigate the Al/Si disorder in silicates and briefly reported their simulated Holl-I structure at zero pressure only. To the contrary, Mookherjee and Steinle-Neumann (2009a) carried out a detailed investigation for a large range of pressure on the elasticity and phase stability of Holl-I and Holl-II. The third study aimed at the elasticity and seismic property of Holl-I (Caracas and Boffa Ballaran 2010). On the other hand, some theoretical calculations have also been made to explore the effect of Na (Boffa Ballaran et al. 2009; Caracas and Boffa Ballaran 2010) that suggested the replacement of K by Na decreases the phase-transition pressure between Holl-I and Holl-II. Here we used a constant pressure ab initio technique to further explore the structural evolution with pressure of Holl-I and Holl-II and the features of the phase transition associated with them.

Details of simulation

Our first-principles simulations were performed by the CASTEP code using density functional theory (DFT) and planewave pseudopotential technique (Payne et al. 1992). We adopted the generalized gradient approximation (GGA) incorporated with the Perdew-Burke-Ernzerhof (PBE) exchange-correlation functional (Perdew et al. 1996). The same theoretical techniques have been used in our previous studies and found to be very powerful in studying the structure and thermodynamics of silicate minerals at high pressures (Deng et al. 2006, 2009, 2010).

More specifically to this study, a planewave basis set with a cutoff of 380 eV was used to expand the electronic wave functions and ultrasoft pseudopotentials were employed to model the ion-electron interaction (Vanderbilt 1990). The irreducible Brillouin zone was sampled by a $3 \times 3 \times 5$ Monkhorst-Pack grid (Monkhorst and Pack 1976). We applied both symmetry constraint and non-symmetry constraint to the simulated cell during the structure relaxation, and reached almost identical results. The neglection of symmetry constraints did not lead to any increase of the computing cycles, but did increase the computing time by ~60%. Equilibrium lattice parameters and internal coordinates were optimized by minimizing the Hellmann-Feynman force on the atoms and simultaneously matching the stress on the unit cell to the target stress. After the final self-consistency cycle, the remaining Hellmann-Feynman forces on the atoms were typically <0.001 eV/Å and the remaining stress was <0.004 GPa. The geometry optimizing was conducted from 0 to 130 GPa at 0 K.

We used the tetragonal hollandite structure (space group *I*4/*m*) as the starting structure in our simulation (Ringwood et al. 1967; Yamada et al. 1984; Zhang et al. 1993). Our computational cell contains 26 atoms. With two of the eight Si atoms in the computational cell replaced by two Al atoms, the tetragonal symmetry degenerates to a monoclinic symmetry. This phenomenon is well known to the scientists in the simulation research field. Different Al/Si substitution mechanisms have been thoroughly examined for zero pressure, and the resulting structures suggest an averaged tetragonal symmetry. In addition, we arbitrarily selected one of the Al/Si substitution mechanisms to probe the structure evolution of Holl-I and Holl-II as pressure increases.

Results and discussions

Effect of different Al/Si substitution mechanisms on the structure of Holl-I at zero pressure

There are eight possible sites for Al and Si in the computing cell (Fig. 1). With the first Al atom (Al-1) taking one of the sites (e.g., site A), the second Al atom (Al-2) can take any of the remaining sites, leading to seven different Al/Si distributions. These seven different configurations have been labeled as A-B, A-C, A-D, A-E, A-F, A-G, and A-H in this study, their respective structural features are listed in Table 1, and their corresponding powder X-ray diffraction patterns are shown in Figure 2.

With the replacement of two Si atoms by two Al atoms, the tetragonal symmetry of Holl-I is lowered to the monoclinic symmetry (Table 1), as illustrated by the various space groups derived from our simulation. Only a very small difference of the unit-cell parameters *a* and *b* (less than about 1%) and a deviation of the γ-angle from 90° (less than about 1°) are responsible for the monoclinic distortion. The fluctuation of the unit-cell parameters caused by the different Al/Si configurations is very small, as suggested by the averaged values of the unit-cell parameters (Table 1). Since the arithmetical averages of the unit-cell parameters show that *a* is essentially equal to *b* and γ close to 90°, we can reasonably assume that the averaged calculated crystal structure is tetragonal, so that the structure of Holl-I has been well simulated in our investigation.

Different Al/Si substitution mechanisms also cause some fluctuation of the cohesive energies (Table 1): the A-B Al/Si configuration leads to the highest value, the A-E and A-F Al/Si distributions result in the lowest values, and all the other four Al/Si configurations attain their cohesive energy values in-between. Nevertheless, the difference between the highest value and the lowest value of the cohesive energy is obviously very small (about 0.9 eV for 26 atoms). Additionally, the small deviation (about 0.1 eV for 26 atoms) of the cohesive energies caused by the different Al/Si distributions indicates that no individual Al/Si

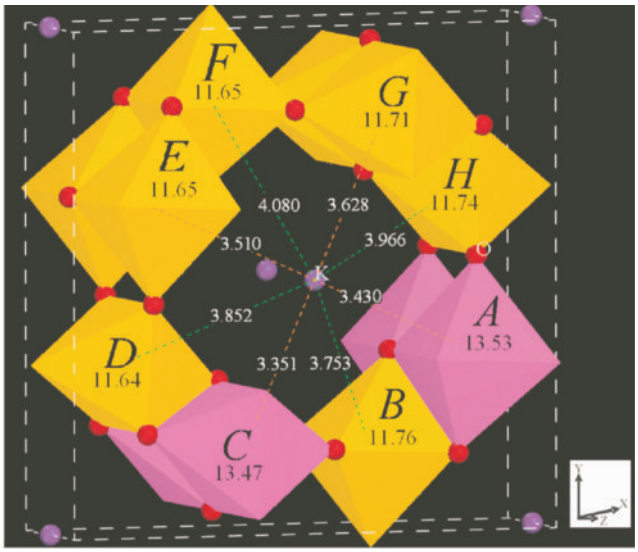

FIGURE 1. Stereoscopic view of Holl-I. Atoms K and O are labeled by their element symbols, while atoms Si and Al, residing in the (Si,Al)O_6 octahedra, are alphabetically labeled from A to H. Octahedra A and C are arbitrarily designated as the AlO_6 octahedra. Numbers shown are for the volume of the (Si,Al)O_6 octahedron (Å^3) or for the bond length of the Si(Al)-K bond (Å). The average volume of the AlO_6 octahedra is generally larger than that of the SiO_6 octahedra by about 15%, whereas the average bond length of Al-K is generally shorter than that of Si-K by about 5% (Z = 1/2; bonds in orange).

TABLE 1. Simulated lattice parameters and minimized cohesive energy (E) for different Al-Si configurations (symmetry constraint-free; 0 K and 0 GPa)

1-2*	a (Å)	b (Å)	c (Å)	α (°)	β (°)	γ (°)	E (eV)	Derived SG†
A-B	9.50	9.44	2.74	90	90	89.0	–9337.5‡	$P2_1/m$
A-C	9.48	9.43	2.75	90	90	89.9	–9338.1‡	Pm
A-D	9.47	9.48	2.74	90	90	90.2	–9337.9‡	Pm
A-E	9.51	9.41	2.74	90	90	88.9	–9338.5‡	$P2/m$
A-F	9.50	9.41	2.75	90	90	88.8	–9338.4‡	Cm
A-G	9.43	9.48	2.75	90	90	90.1	–9338.1‡	Pm
A-H	9.47	9.48	2.74	90	90	90.2	–9337.9‡	Pm
Mean	9.48(3)	9.45(3)	2.74(1)	90(0)	90(0)	89.6(6)	–9338.1(1)‡	$I4/m$?

* Position of Al-1 vs. that of Al-2, as shown in Figure 1.
† Derived space group.
‡ Value for 26 atoms.

distribution is dominant, which is in good agreement with Post and Burnham (1986) and Caracas and Boffa Ballaran (2010).

The calculated powder X-ray diffraction patterns for the different Al/Si distributions are shown in Figure 2 and compared to experimentally obtained powder X-ray patterns for Holl-I and Holl-II (Zhang et al. 1993; Sueda et al. 2004). In general, the powder X-ray patterns for the A-H and A-D Al/Si configurations are very similar and approximate that of Holl-I. All other powder X-ray patterns, on the other hand, have not been observed experimentally for Holl-I. In particular, the powder X-ray patterns for the A-B, A-E, and A-F Al/Si distributions show some features, as denoted by the asterisks, that actually belong to Holl-II only. Consequently, the arithmetic average of the calculated powder X-ray diffraction patterns should not be expected to resemble the experimentally observed powder X-ray diffraction pattern of Holl-I (Zhang et al. 1993), which is the case indeed (Fig. 3).

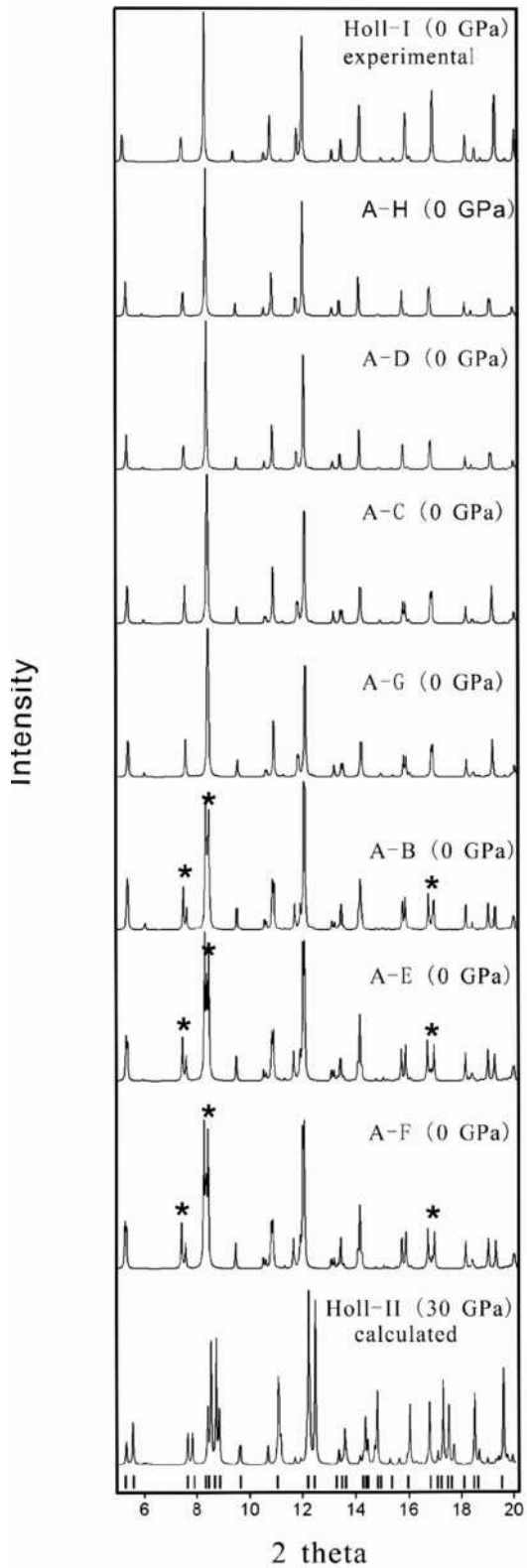

FIGURE 2. Computed powder X-ray diffraction patterns of Holl-I with different Al/Si distributions (0 K and 0 GPa; λ = 0.4258 Å). For the purpose of comparison, the experimentally obtained powder X-ray diffraction pattern of Holl-I [room T and 0 GPa; Zhang et al. (1993)], simulated powder X-ray diffraction pattern of Holl-II (0 K and 30 GPa; this study), and experimentally determined peak positions of Holl-II [room T and 27.5 GPa; Sueda et al. (2004)] are also plotted.

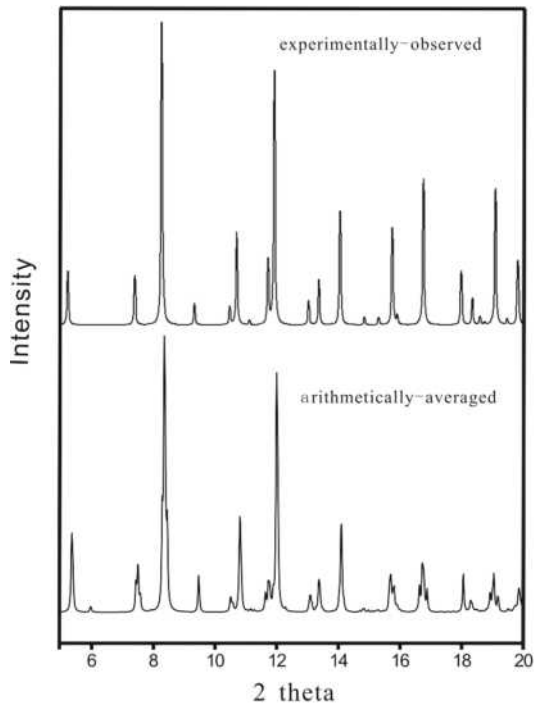

FIGURE 3. Comparison of arithmetically averaged powder X-ray diffraction pattern to experimentally obtained powder X-ray diffraction pattern of Holl-I. Note the peak splitting in the averaged powder X-ray diffraction pattern.

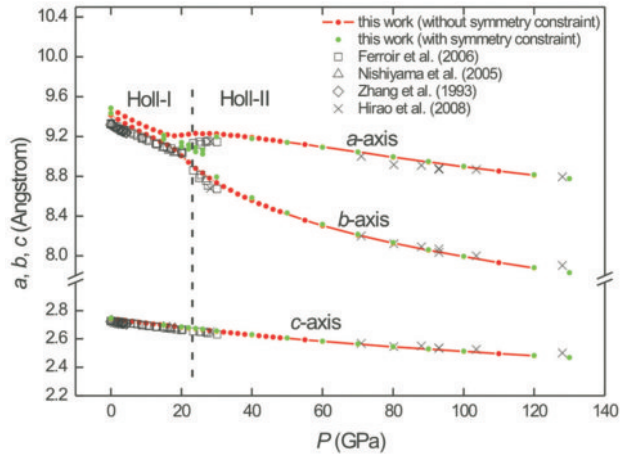

FIGURE 4. Variation of unit-cell parameters *a*, *b*, and *c* with pressure (A-C Al/Si configuration). Discontinuities in the *a*- and *b*-axes associated with the phase transition from Holl-I to Holl-II are indicated by the broken line at around 23 GPa. On the other hand, no discontinuity is observed for the *c*-axis.

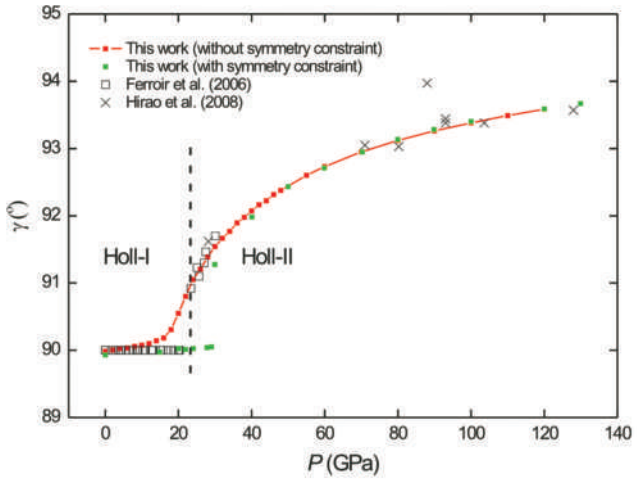

FIGURE 5. Variation of unit-cell parameter γ with pressure (A-C Al/Si substitution mechanism). The phase transition from Holl-I to Holl-II is indicated by the broken line at around 23 GPa.

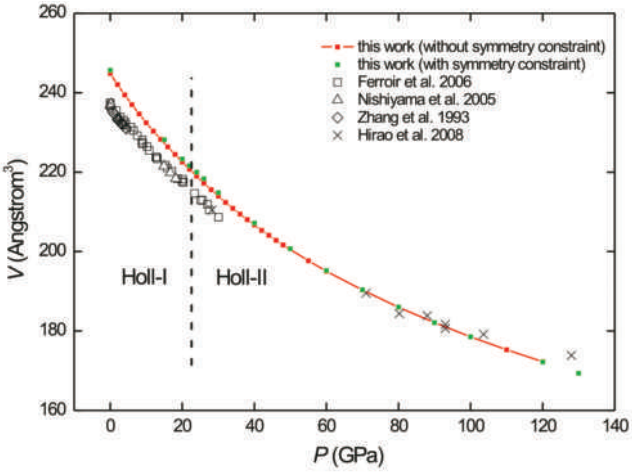

FIGURE 6. Variation of unit-cell volume with pressure (A-C Al/Si substitution mechanism). No apparent volume discontinuity has been observed at around 23 GPa.

It follows that in the real Holl-I crystal structure some Al/Si distributions such as A-H and A-D should be more important than others, suggesting that some local Al-Si ordering does exist to some extent. This argument should be further strengthened by any potential effect of temperature, which in general promotes Al-Si disordering. Since the different Al/Si substitution mechanisms do not result in much difference in the cohesive energy, other factors like charge neutralization and spatial requirement must be taken into consideration to account for the potential non-random distribution of Al and Si.

Structural evolution and phase transition of Holl-I and Holl-II

The A-C Al/Si distribution was arbitrarily selected to probe the structural evolution of the hollandites at high pressures. As shown in Figures 4, 5, and 6, intensive simulation points were arranged, with a step size of 2 GPa between 0 and 50 GPa and a step size of 5 or 10 GPa between 50 and 130 GPa.

As shown in Figure 4, the small difference between the unit-cell parameters *a* and *b* (~0.5%; a result of the special Al/Si substitution mechanism) maintains at least up to about 18 GPa (symmetry-unconstrained cell) or 28 GPa (symmetry-constrained cell), from where it starts to increase quickly. Within a pressure interval of about 4 GPa (22 GPa for the case without symmetry constraint or 32 GPa for the case with symmetry constraint), the difference between *a* and *b* sharply increases to about 5%, a value, which cannot be accounted for by any other factor

but a phase transition. As mentioned above, the different Al/Si configurations result in differences in *a* and *b* of maximal 1% (Table 1; 0 GPa). Furthermore, Figure 4 shows no abrupt change for the *c*-axis.

Figure 5 shows that with the symmetry-unconstrained cell, the deviation of the γ-angle from 90° is limited to about 0.3° as pressure increases from 0 to 18 GPa, but quickly increases to about 0.8° at 22 GPa. For the symmetry-constrained cell, the deviation is about 0.04° at 28 GPa, but about 1.5° at 32 GPa. This phenomenon strongly suggests a phase transition as well.

On the other hand, Figure 6 shows that the evolution of the unit-cell volume with pressure does not show any apparent discontinuity.

Existing in situ high-*P* experiments demonstrated that the phase transition from Holl-I to Holl-II at about 23 GPa was a second-order phase transition characterized by the splitting of the *a*-axes into a long *a*- and a short *b*-axis, rapid deviation of the γ-angle from 90°, and unobservable volume discontinuity (Nishiyama et al. 2005; Ferroir et al. 2006; Hirao et al. 2008). The theoretical calculations reported here have successfully reproduced all major features associated with this phase transition (Figs. 4, 5, and 6). Considering the strong similarity between the simulated results and experimental observations, we tend to believe that the phase transition captured by our simulation is indeed the phase transition from Holl-I to Holl-II, and the phase transition takes place at about 23(5) GPa.

The structural evolution of Holl-I with pressure was evaluated both by high-*P* compression experimentation and theoretical simulation (Nishiyama et al. 2005; Ferroir et al. 2006; Mookherjee and Steinle-Neumann 2009a). Our simulated unit-cell parameters at $P \le 16$ GPa (symmetry-unconstrained cell) generates the following empirical equations:

$a = 9.470(5) - 0.0165(5)P$ ($R^2 = 0.9933$)
$b = 9.407(2) - 0.0185(3)P$ ($R^2 = 0.9987$)
$c = 2.74353(3) - 0.00340(1)P + 0.0000192(6)P^2$ ($R^2 = 1.0000$)
$\gamma = 89.99(1) + 0.004(2)P + 0.0005(1)P^2$ ($R^2 = 0.9886$)
$V = 244.81(3) - 1.382(9)P + 0.0144(5)P^2$ ($R^2 = 1.0000$)
$c/a = 0.28938(2) + 0.00029(1)P - 0.0000069(3)P^2$ ($R^2 = 0.9996$)
$c/b = 0.29149(4) + 0.00028(1) - 0.0000017(8)P^2$ ($R^2 = 0.9988$)

where *a*, *b*, and *c* are in angstroms, *P* is in GPa, *V* is in cubic angstroms, and γ is in degrees. Since the *a*/*b* ratios at different pressures are close to 1 and very constant [1.008(1)], it is reasonable to use the average (*a*) of *a* and *b* to derive an empirical equation to simultaneously describe the evolution of both *a* and *b* at high pressures: $a = 9.446(1) - 0.0209(2)P + 0.00022(1)P^2$ ($R^2 = 1.0000$). In turn, the *c*/*a* ratio at different pressures can be empirically described by $c/a = 0.29043(2) + 0.000286(5)P - 0.0000043(3)P^2$ ($R^2 = 1.0000$).

For the Holl-I structure, apparently, the elastic anisotropy along the *a*-axis and *c*-axis increases with pressure increase, confirming previous experimental observations (Zhang et al. 1993; Nishiyama et al. 2005).

In comparison, high-*P* experiments were previously carried out with the Holl-II phase at pressures either below 30 GPa or above 70 GPa only (Nishiyama et al. 2005; Ferroir et al. 2006; Hirao et al. 2008), so that a full description of the structure evolution of Holl-II with pressure was not possible. Our theoretical work has filled the pressure gap of 30–70 GPa and provided a good opportunity to probe the evolution with pressure of the lattice parameters of Holl-II. With the data from our simulations at $P \ge 30$ GPa (symmetry-unconstrained cell), we have reached some empirical equations as following:

$a = 9.377(2) - 0.00477(4)P$ ($R^2 = 0.9990$)
$b = 9.247(23) - 0.0200(7)P + 0.000073(5)P^2$ ($R^2 = 0.9979$)
$c = 2.736(1) - 0.00295(4)P + 0.0000071(3)P^2$ ($R^2 = 0.9999$)
$\gamma = 90.12(9) + 0.058(3)P - 0.00025(2)P^2$ ($R^2 = 0.9943$)
$V = 236.21(54) - 0.837(18)P + 0.00256(12)P^2$ ($R^2 = 0.9995$)
$a/b = 1.009(3) + 0.0019(1)P - 0.0000088(8)P^2$ ($R^2 = 0.9912$)
$c/a = 0.2919(4) - 0.00017(1)P + 0.0000008(1)P^2$ ($R^2 = 0.9891$)
$c/b = 0.2949(6) + 0.00037(2)P - 0.0000017(1)P^2$ ($R^2 = 0.9914$)

where *a*, *b*, and *c* are in angstroms, *P* is in GPa, *V* is in cubic angstroms, and γ is in degrees. For Holl-II, the correlation between the *c*/*a* ratio and *P* is negative, whereas that of the *c*/*b* ratio and *P* is positive; for Holl-I, in contrast, both correlations are positive. This confirms the experimental observations made by Hirao et al. (2008).

Equation of state (EoS) of Holl-I and Holl-II

The isothermal bulk modulus K_0 and its first derivative K_0' can be derived by fitting the calculated *P*-*V* data to the third-order Birch-Murnaghan equation of state (BM-EoS; Birch 1978)

$$P = \frac{3}{2} K_0 [(\frac{V_0}{V})^{7/3} - (\frac{V_0}{V})^{5/3}] \{1 - \frac{3}{4}(4 - K_0^{'})[(\frac{V_0}{V})^{2/3} - 1]\}$$

in which K_0 is the isothermal bulk modulus at zero pressure, K_0' is the first derivative of K_0, V_0 is the volume at zero pressure, and *V* is the volume at high pressure. To derive the EoS of Holl-I and Holl-II, we used the *P*-*V* data from 0 to 20 GPa for Holl-I and those from 30 to 130 GPa for Holl-II (A-C Al/Si configuration; symmetry-unconstrained cell; 0 K). The final EoS parameters are listed and compared with the literature data in Table 2.

The experimentally determined K_0 for Holl-I varies between 180 and 201 GPa, with similar values of V_0 derived ($K_0' = 4$; Zhang et al. 1993; Nishiyama et al. 2005; Ferroir et al. 2006). Our theoretical work (GGA) suggested a V_0 about 3% larger than the experimentally determined values and a slightly smaller K_0 of 174 GPa, which is close to the low value determined in the high-*P* experiments. In comparison, the theoretical work (LDA) done by Mookherjee and Steinle-Neumann (2009a) generated a V_0 about 4% smaller than the experimentally determined values and a slightly larger K_0 of 225 GPa, which is close to the high value determined in the high-*P* experiments. Clearly, this discrepancy in K_0 is mainly caused by the difference in the investigation methods: GGA leads to slightly overestimated unit-cell volume, whereas LDA leads to slightly underestimated unit-cell volume; this phenomenon is especially pronounced at low pressures.

There has not been reliable experimental determination of the K_0 of Holl-II. Hirao et al. (2008) did the pioneering work and provided the first number, which was unfortunately affected by the unavailability of the *P*-*V* data between 30 and 70 GPa. On the other hand, the theoretical work in this study (GGA) and that

TABLE 2. EoS parameters of Holl-I and Holl-II for the composition of $KAlSi_3O_8$

V_0 (Å^3)	K_0 (GPa)	K_0'	Reference
		Holl-I	
244.82	174.02	3.99	This work*
227.65	225.0	4.3	Mookherjee and Steinle-Neumann (2009a)*
228.17	224	–	Caracas and Boffa Ballaran (2010)*
236.26(36)†	180(3)	4‡	Zhang et al. (1993)
237.6(2)	183(3)	4‡	Nishiyama et al. (2005)
237.01(33)	201.4(7)	4‡	Ferroir et al. (2006)
241.06	–	–	Ringwood et al. (1967)
236.73	–	–	Yamada et al. (1984)
		Holl-II	
244.8	168.2	4‡	This work*
228.02	220.5	3.9	Mookherjee and Steinle-Neumann (2009a)*
232.3(22)	232(14)	4‡	Hirao et al. (2008)
237.01	181.0	4.9	Mookherjeeand Steinle-Neumann (2009a)§

* Simulated result at 0 K.
† Numbers in parentheses represent one standard deviation.
‡ Value fixed.
§ Experimental data from Ferroir et al. (2006) and Hirao et al. (2008) used to derive the EoS parameters.

in Mookherjee and Steinle-Neumann (2009a; LDA) can provide some constraints on the K_0 of Holl-II: the low boundary should be close to 168 GPa, whereas the high value should be close to 221 GPa (Table 2). It follows that the K_0 value of Holl-II from Hirao et al. [2008; 232(14) GPa] appears too large. Combining the high-P experimental data from Ferroir et al. (2006) and those from Hirao et al. (2008), Mookherjee and Steinle-Neumann (2009a) tentatively suggested a value of 181 GPa, which seems much compatible to the theoretical results.

The EoS of Holl-I and Holl-II can be affected by the replacement of K with Na (Boffa Ballaran et al. 2009; Caracas and Boffa Ballaran 2010). The high-P experiments of Boffa Ballaran et al. (2009) constrained the K_0 of Holl-I and Holl-II in the composition of $K_{0.8}Na_{0.2}AlSi_3O_8$ to 198(3) and 174(7) GPa, respectively. The theoretical investigation of Caracas and Boffa Ballaran (2010) obtained the K_0 of Holl-I of the same composition as 220 GPa. A comparison of these values to those for the composition $KAlSi_3O_8$ listed in Table 2 reveals a potentially small effect of replacing K by Na on the K_0 of Holl-I and Holl-II. Interestingly, the difference in the K_0 values of the phase-X with the compositions of $K_2Mg_2Si_2O_7$ and $Na_2Mg_2Si_2O_7$ is also very small (132 and 128 GPa, respectively; Mookherjee and Steinle-Neumann 2009b). Pressure, however, tends to substantially enhance the effect of composition on the bulk moduli both in the case of Holl-I and Holl-II (Caracas and Boffa Ballaran 2010), and in the case of the phase-X (Mookherjee and Steinle-Neumann 2009b).

Microscopic structural deformation and phase transition mechanism

In the structures of Holl-I and Holl-II, the $(Si,Al)O_6$ octahedra share edges to form double chains parallel to the c-axis, which in turn share corners with neighboring double chains to form a framework structure (Ringwood et al. 1967; Yamada et al. 1984; Zhang et al. 1993; Ferroir et al. 2006; Hirao et al. 2008). Under hydrostatic compression, intuitively, the $(Si,Al)O_6$ octahedra should generally behave as rigid blocks, and so should the double chains of the $(Si,Al)O_6$ octahedra due to their edge-sharing characteristic. The weakest part of the framework is expected to be the shared corners of the double chains, which define the shape and size of the open channel of KO_8. As shown in Figure 7, the $(Si,Al)O_6$ octahedron is indeed much less compressible than the KO_8 polyhedron. Specifically, the K_0 of the AlO_6 is 246 GPa, that of SiO_6 is 302 GPa, and that of KO_8 is 193 GPa (K_0' fixed at 4; BM-EoS). These values are well in line with the results of Mookherjee and Steinle-Neumann (2009a; 259, 342, and 157 GPa, respectively), taking into account the difference in the simulating techniques [GGA in this study while LDA in Mookherjee and Steinle-Neumann (2009a)]. Experimentally, Zhang et al. (1993) proposed that the KO_8 polyhedron in the Holl-I phase is much less compressible than the $(Si,Al)O_6$ octahedron, whereas Hirao et al. (2008) claimed the opposite for the Holl-II phase. Since the K-O bond is generally regarded as one of the most compressible bonds among the metal-oxygen pairs in oxide minerals (Hazen and Prewitt 1977), the observation made in Zhang et al. (1993) appears unlikely. There were two major factors, which may explain this peculiarity: first, the maximum pressure in the experiments of Zhang et al. (1993) was limited to 4.47 GPa, which is apparently too low for a high-quality EoS investigation; second, the errors of the volume data for the rigid $(Si,Al)O_6$ octahedron were claimed to be very large, but unfortunately not reported and used in the BM-EoS fitting, leading to significant underestimation of the error of the bulk modulus.

Rigid as they may be, under hydrostatic compression, the $(Si,Al)O_6$ octahedra not only reduce their volumes, but change their shapes as well (Fig. 8a). The evolution with pressure of the angle depicted in Figure 8a indicates that the octahedron becomes more shortened along the y-axis. Additionally, no apparent discontinuity has been observed during the deformation of the $(Si,Al)O_6$ octahedron, suggesting the phase transition of Holl-I and Holl-II must be trigged by other mechanisms.

As outlined above, the corners shared by the neighboring double chains are expected to be the weakest part of the framework structure of Holl-I and Holl-II. The evolution with pressure of one of the hinge angles between the neighboring double chains is shown in Figure 8b: it decreases slowly from 0 to about 18 GPa, drops quickly in the pressure interval of 18–28 GPa, and

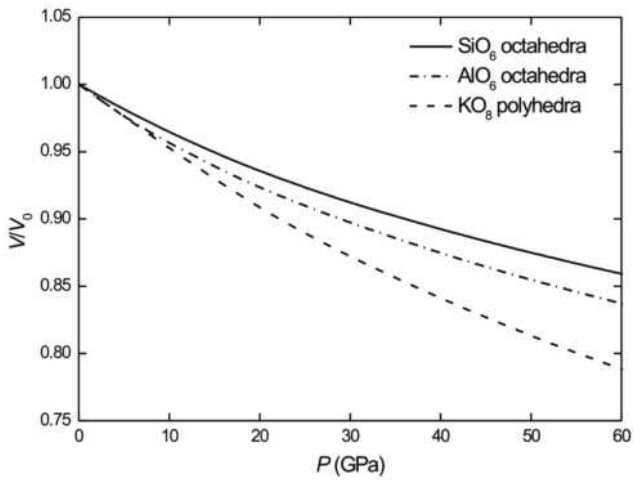

FIGURE 7. Evolution of KO_8 polyhedra, SiO_6 octahedra, and AlO_6 octahedra with increasing pressure (A-C Al/Si configuration; symmetry-unconstrained cell). Averaged volume of SiO_6 octahedra B, D, E, F, G, and H or that of AlO_6 octahedra A and C is plotted (see Fig. 1 for more information).

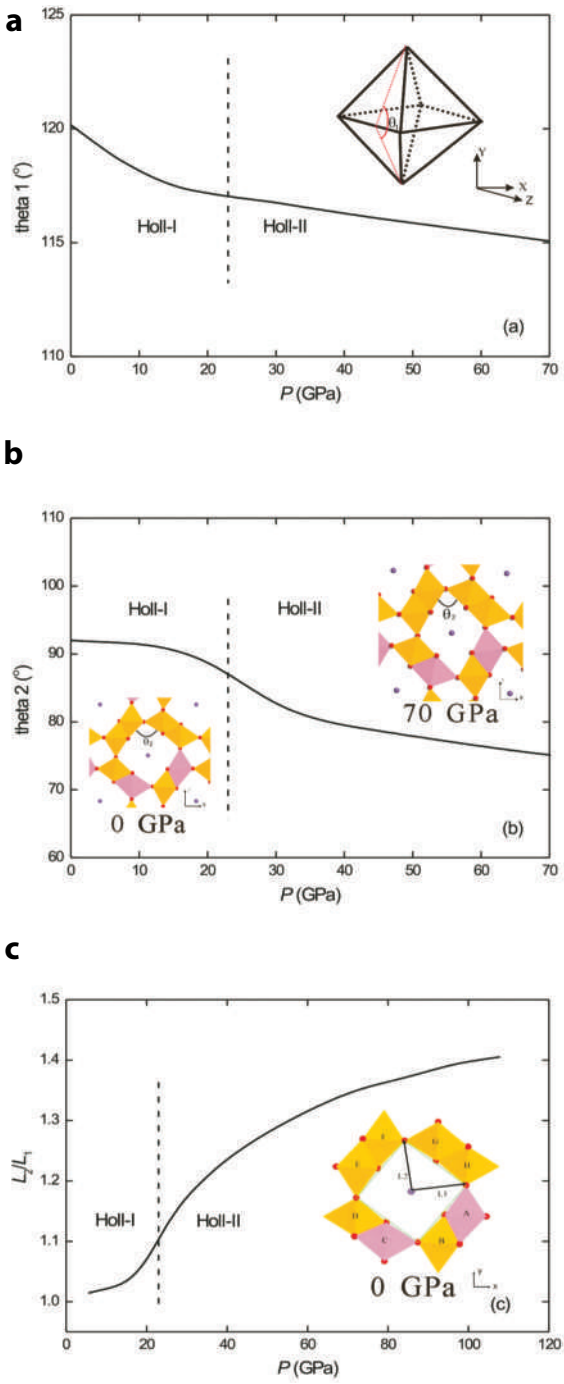

FIGURE 8. Microscopic structural deformation as pressure increases (A-C Al/Si configuration; symmetry-unconstrained cell): (**a**) deformation of the SiO_6 octahedron exampled by octahedron *E*; (**b**) evolution of one of the hinge angles; (**c**) dimensional evolution of the open channel.

reduces slowly again at higher pressures. It is believed that this response of the hinge angles to the change of pressure is the most likely cause to the phase transition of Holl-I to Holl-II. Due to the change of the hinge angles at high pressures, the shape of the open channel changes accordingly: the L_2/L_1 ratio increases slowly from 0 to about 18 GPa, quickly in the pressure interval of 18–28 GPa, and slowly again at higher pressures (Fig. 8c).

With the discussion above, we can start to pursue the phase transition mechanism from Holl-I to Holl-II. If Al-1 resides in the octahedron A, Al-2 accordingly resides in the octahedron H, D, C, or G as indicated by the similarity between the experimentally observed powder X-ray diffraction data and our simulated powder X-ray diffraction patterns for Holl-I (Fig. 2). Since the minimized cohesive energy for the A-C or A-G Al/Si configuration is slightly smaller than that for the A-D or A-H Al/Si distribution (Table 1), the most likely site for Al-2 is the octahedron C or G. Whichever octahedron Al-2 enters, the Al-$1O_6$ octahedron and Al-$2O_6$ octahedron are on neighboring double chains and separated by only one SiO_6 octahedron. Due to charge balance, the K cation is offset from the *c*-axis and closer to the two AlO_6 octahedra (Fig. 1); indeed, the average K-Al bond is shorter than the average K-Si bond by about 5%. The most diagnostic direction of the displacement of the K cation from the *c*-axis, apparently, is from the octahedron B to octahedron F, with the K cation about 8% closer to the octahedron B (using the A-C Al/Si substitution mechanism as an example). Since the AlO_6 octahedra are more compressible than the SiO_6 octahedra, the space where the K cation resides at low pressure will be slowly reduced by pressure increase, and the K cation will be slowly pushed toward the *c*-axis. Along with this process are the minor reduction of the hinge angle between those two AlO_6-bearing double chains (Fig. 8b) and the dimensional change of the open channel (Fig. 8c). Due to charge neutralization and spatial requirement, the process might stop as the transition pressure from Holl-I to Holl-II approaches, and further pressure increase perhaps make Al-2 change its position to the octahedron E or F. When that takes place, the powder X-ray diffraction pattern then will have the diagnostic signals of Holl-II (Fig. 2). Although the powder X-ray diffraction pattern of the A-B Al/Si substitution mechanism also shows the features of Holl-II, the octahedron B is apparently a very bad candidate, which leads to an unbalanced structure. This phase transition mechanism is generally supported by the direct experimental observations using synchrotron X-ray radiation: at different temperatures, peak broadening and splitting were not observed at pressures far from the transition pressures from Holl-I to Holl-II but at pressures near the phase transition (Sueda et al. 2004; Nishiyama et al. 2005; Ferroir et al. 2006).

Geochemical implication

In general, hollandite-type compounds possess a common chemical formula $A_xB_8O_{16}$, where A represents large mono- or divalent cations with $x \leq 2$, and B represents smaller, two- to five-valent cations. Some previous investigations proposed that the cell volume of the hollandites is completely dependent on the $Si(Al)O_6$ octahedron, since the AO_8 polyhedron behaves as a rigid body (Post et al. 1982; Cheary 1986). Therefore, the size of the A cation is a relatively unimportant factor, and a large variety of chemical species (such as K, Ag, Ba, Rb, and Cs) can be readily accommodated by the hollandite structure. This might be true for the $KAlSi_3O_8$ Holl-I, which is stable at relatively low pressures, as indicated by the high-*P* experiments of Rapp et al. (2008). In the case of the $KAlSi_3O_8$ Holl-II, however, our simulation has demonstrated that its KO_8 polyhedron is much more compressible than the $Si(Al)O_6$ octahedron, which in turn means that the size of the A cation will become very important

as pressure increases. Therefore, it will become much more difficult for those large-radius cations (like Rb and Cs) to occupy the tunnel site, especially under high pressures, where the tunnel might even be fully collapsed. When that happens, a new phase or phase assemblage will form for the composition $KAlSi_3O_8$.

It has been documented that, with or without Holl-I as part of the phase assemblage, the partitioning behaviors of trace elements between the solid phase assemblage and silicate melt are quite different in the partially molten subducted sediments (Rapp et al. 2008; Beck et al. 2005), which has been regarded as a geochemically distinct magma reservoir in the deep mantle (Zindler and Hart 1986). As demonstrated by the experimental studies in the literature and the first-principles simulation here, however, the phase transition from Holl-I to Holl-II taking place at ~23(5) GPa results in some distinct crystal structural modification, especially the shape and dimension of the open channel, which hosts the large radius cations. Consequently, the phase transition from Holl-I to Holl-II might have significant effects on the partitioning of the trace elements between the solid phase assemblage and the melt. So far no data about the partitioning of the trace element between Holl-II and silicate melt are available, and more high-*P* experiments are apparently needed.

Acknowledgments

The authors thank Y. Fei, Z. Gong, L. Zhang, and H. Zhen for providing valuable suggestions and comments on the project, and M. Mookherjee and one anonymous reviewer for their constructive comments, which substantially improved the manuscript. The authors are also grateful to S. Redfern for his editorial help and scientific suggestions. This study was financially supported by the National Natural Science Foundation of China (Grant 40872033).

References cited

Akaogi, M., Kamii, N., Kishi., A., and Kojitani, H. (2004) Calorimetric study on high pressure transitions in $KAlSiO_3$. Physics and Chemistry of Minerals, 31, 85–91.

Beck, P., Gillet, Ph., El Goresy, A., and Mostefaoul, S. (2005) Timescales of shock processes in chondritic and Martian meteorites. Nature, 435, 1071–1074.

Birch, F. (1978) Finite strain isotherm and velocities for single-crystal and polycrystalline NaCl at high pressures and 300 K. Journal of Geophysical Research, 83, 1257–1268.

Boffa Ballaran, T., Liu, J., Dubrovinsky, L.S., Caracas, R., and Crichton, W. (2009) High-pressure ferroelastic phase transition in aluminosilicate hollandite. Physical Review B, 80, 214104.

Bozhilov, K.N., Green, H.W. II, and Dobrzhinetskaya, L.F. (1999) Clinoenstatite in Alpe Arami peridotite: additional evidence of very high pressure. Science, 284, 128–132.

Caracas, R. and Boffa Ballaran, T. (2010) Elasticity of $(K,Na)AlSi_3O_8$ hollandite from lattice dynamics calculations. Physics of the Earth and Planetary Interiors, 181, 21–26.

Cheary, R.W. (1986) An analysis of the structural characteristics of hollandite compounds. Acta Crystallographica, B42, 229–236.

Deng, L., Zhao, J., Ji, G., Gong, Z., and Wei, D. (2006) First-principles study of orthorhombic perovskites $MgSiO_3$ up to 120 GPa and its geophysical implications. Chinese Physics Letters, 23, 2334–2337.

Deng, L., Zhao, J., Liu, H., Wu, D., and Gong, Z. (2009) Pressure-related phase stability of $MgSiO_3$ and $(Mg_{0.75},Fe_{0.25})SiO_3$ at lower mantle condition. International Journal of Modern Physics B, 23, 3323–3329.

Deng, L., Liu, X., Liu, H., and Dong, J. (2010) High-pressure phase relations in the composition of albite $NaAlSi_3O_8$ constrained by an ab initio and quasi-harmonic Debye model, and their implications. Earth and Planetary Science Letters, 298, 427–433.

Dupre, B. and Allegre, C.J. (1983) Pb-Sr isotope variation in Indian ocean basalts and mixing phenomena. Nature, 303, 142–146.

Durandurdua, M. (2009a) Pressure-induced phase transition in AlN: An ab initio molecular dynamics study. Journal of Alloys and Compounds, 480, 917–921.

——— (2009b) Pressure-induced phase transition in wurtzite ZnS: An ab initio constant pressure study. Journal of Physics and Chemistry of Solids, 70, 645–649.

Ferroir, T., Onozawa, T., Yagi, T., Merkel, S., Miyajima, N., Nishiyama, N., Irifune, T., and Ikegawa, T. (2006) Equation of state and phase transition in $KAlSi_3O_8$ hollandite at high pressure. American Mineralogist, 91, 327–332.

Hazen, R.M. and Prewitt, C.T. (1977) Effects of temperature and pressure on interatomic distances in oxygen-based minerals. American Mineralogist, 62, 309–315.

Hirao, N., Ohtani, E., Kondo, T., Sakai, T., and Kikegawa, T. (2008) Hollandite II phase in $KAlSi_3O_8$ as a potential host mineral of potassium in the Earth's lower mantle. Physics of the Earth and Planetary Interiors, 166, 97–104.

Hirose, K., Fei, Y., and Mao, H.K. (1999) The fate of subducted basaltic crust in the Earth's lower mantle. Nature, 397, 53–56.

Hofmann, A.W. (1997) Mantle geochemistry: The message from oceanic volcanism. Nature, 385, 219–229.

Iitaka, T., Hirose, K., Kawamura, K., and Murakami, M. (2004) The elasticity of the $MgSiO_3$ post-perovskite phase in the Earth's lowermost mantle. Nature, 430, 442–445.

Irifune, T., Ringwood, A.E., and Hibberson, W.O. (1994) Subduction of continental crust and terrigenous and pelagic sediments: an experimental study. Earth and Planetary Science Letters, 126, 351–368.

Liu, L. and El Goresy, A. (2007) High-pressure phase transitions of the feldspars and further characterization of lingunite. International Geology Review, 49, 854–860.

Liu, L., Zhang, J., Green, H.W. II, Jin, Z., and Bozhilov, K.N. (2007) Evidence of former stishovite in metamorphosed sediments, implying subduction to >350 km. Earth and Planetary Science Letters, 263, 180–191.

Liu, L., Lin, C.C., Yung, Y.J., Mernagh, T.P., and Irifune, T. (2009) Raman spectroscopic study of K-lingunite at various pressures and temperatures. Physics and Chemistry of Minerals, 36, 143–149.

Liu, X. (2006) Phase relations in the system $KAlSi_3O_8$-$NaAlSi_3O_8$ at high pressure-high temperature conditions and their implication for the petrogenesis of lingunite. Earth and Planetary Science Letters, 246, 317–325.

Liu, X., Hu, Z., and Deng, L. (2010) Feldspars under conditions of high temperature-high pressure. Acta Petrologica Sinica, 26, 3601–3610.

Martinez, I. and Durandurdua, M. (2006) Ab initio molecular dynamics study of pressure-induced phase transition in ZnS. Journal of Physics: Condensed Matter, 18, 9483–9491.

Meng, S., Wang, E.G., and Gao, S.W. (2004) The pressure induced phase transition of confined water from ab initio molecular dynamics simulation. Journal of Physics: Condensed Matter, 16, 8851–8859.

Monkhorst, H.J. and Pack, J.D. (1976) Special points for Brillouin-zone integrations. Physical Review B, 13, 5188–5192.

Mookherjee, M. and Steinle-Neumann, G. (2009a) Detecting deeply subducted crust from the elasticity of hollandite. Earth and Planetary Science Letters, 288, 349–358.

——— (2009b) Elasticity of phase-X at high pressure. Geophysical Research Letters, 36, L08307.

Nishiyama, N., Rapp, R.P., Irifune, T., Sanehira, T., Yamazaki, D., and Funakoshi, K. (2005) Stability and P-V-T equation of state of $KAlSi_3O_8$-hollandite determined by in situ X-ray observations and implications for dynamics of subducted continental crust material. Physics and Chemistry of Minerals, 32, 627–637.

Payne, M.C., Teter, M.P., Allan, D.C., Arias, T.A., and Joannopoulos, J.D. (1992) Iterative minimization techniques for ab initio total-energy calculations: molecular dynamics and conjugate gradients. Reviews of Modern Physics, 64, 1045–1097.

Perdew, J.P., Burke, K., and Ernzerhof, M. (1996) Generalized gradient approximation made simple. Physical Review Letters, 77, 3865–3868.

Post, J.E. and Burnham, C.W. (1986) Modelling tunnel-cation displacements in hollandites using structure-energy calculations. American Mineralogist, 71, 1178–1185.

Post, J.E., Von Dreele, R.B., and Buseck, P.R. (1982) Symmetry and cation displacements in hollandites: Structure refinements of hollandite, cryptomelane and periderite. Acta Crystallographica, B38, 1056–1065.

Rapp, R.P., Irifune, T., Shimizu, N., Nishiyama, N., Norman, M.D., and Inoue, T. (2008) Subduction recycling of continental sediments and the origin of geochemically enriched reservoirs in the deep mantle. Earth and Planetary Sciences Letters, 271, 14–23.

Ringwood, A.E., Fredi, A.F., and Wadsley, A.D. (1967) High-pressure $KAlSi_3O_8$ and aluminosilicate with sixfold coordination. Acta Crystallographica, 23, 1093–1095.

Sueda, Y., Irifune, T., Nishiyama, N., Rapp, R.P., Ferroir, T., Onozawa, T., Yagi, T., Merkel, S., Miyajima, N., and Funakoshi, K.I. (2004) A new high-pressure form of $KAlSi_3O_8$ under lower mantle conditions. Geophysical Research Letters, 31, L23612.

Tutti, F., Dubrovinsky, L.S., Saxena, S.K., and Carlson, S. (2001) Stability of $KAlSi_3O_8$ Hollandite-type structure in the Earth's lower mantle conditions. Geophysical Research Letters, 28, 2735–2738.

Urakawa, S., Kondo, T., Igawa, N., Shimomura, O., and Ohno, H. (1994) Synchrotron radiation study on the high-pressure and high-temperature phase relations of $KAlSi_3O_8$. Physics and Chemistry of Minerals, 21, 387–391.

Vanderbilt, D. (1990) Soft self-consistent pseudopotentials in a generalized eigen-

value formalism. Physical Review B, 41, 7892–7895.
Waghmare, U.V. and Rabe, K.M. (1997) Ab initio statistical mechanics of the ferroelectric phase transition in $PbTiO_3$. Physical Review B, 55, 6161–6173.
Winkler, B., Pickard, C., and Milman, V. (2002) Applicability of a quantum mechanical "virtual crystal approximation" to study Al/Si-disorder. Chemical Physics Letters, 362, 266–270.
Wu, Y., Fei, Y., Jin, Z., and Liu, X. (2009) The fate of subducted Upper Continental Crust: An experimental study. Earth and Planetary Science Letters, 282, 275–284.
Yagi, A., Suzuki, T., and Akaogi, M. (1994) High pressure transitions in the system $KAlSi_3O_8$-$NaAlSi_3O_8$. Physics and Chemistry of Minerals, 21, 12–17.
Yamada, H., Matsui, Y., and Ito, E. (1984) Crystal-chemical characterization of $KAlSi_3O_8$ with the hollandite structure. Mineralogical Journal, 12, 29–34.
Yong, W., Dachs, E., Withers, A.C., and Essene, E.J. (2006) Heat capacity and phase equilibria of hollandite polymorph of $KAlSi_3O_8$. Physics and Chemistry of Minerals, 33, 167–177.
Zhang, J.M., Ko, J.D., Hazen, R.M., and Prewitt, C.T. (1993) High-pressure crystal chemistry of $KAlSi_3O_8$ hollandite. American Mineralogist, 78, 493–499.
Zindler, A. and Hart, S.R. (1986) Chemical geodynamics. Annual Review of Earth and Planetary Sciences, 14, 493–571.

Manuscript received September 12, 2010
Manuscript accepted March 3, 2011
Manuscript handled by Simon Redfern